JOURNAL OF MATERIALS SCIENCE **35** (2000) 1707–1714

Characterization of plasma nitrided pure titanium by X-ray absorption spectroscopy

V. G. PALSHIN, E. I. MELETIS
Louisiana State University, Mechanical Engineering Department, Materials Science and Engineering Program, Baton Rouge, Louisiana

P. J. SCHILLING, R. C. TITTSWORTH
Louisiana State University, Center for Advanced Microstructures and Devices, Baton Rouge, Louisiana

V. M. ADEEV
Institute of Materials Science, Kiev, Ukraine

To date, the exact nature of the plasma nitriding mechanism and the role of energetic particle bombardment are not well understood. The purpose of this work has been to obtain a more detailed knowledge about the evolution of the plasma nitrided surface layer as a function of the energy of the bombarding particles. Nitrided layers were produced at the surface of pure titanium specimens at various flux energies by Intensified Plasma-Assisted Processing (IPAP), a triode plasma technique developed in our laboratory. X-ray Absorption Near Edge Structure (XANES) spectroscopy and Extended X-ray Absorption Fine Structure (EXAFS) spectroscopy were used to characterize the local structure of the titanium nitride layers. Cross sections of the processed specimens were studied by Auger electron spectroscopy and electron microscopy. The results showed that increasing flux energy promotes the formation of a well-ordered TiN layer at the surface. Low flux energies produce significantly lower fractions of the TiN phase at the surface, as well as thinner nitrided layers. A structural model was suggested and quantitatively tested based on the XANES and EXAFS measurements.

1. Introduction

Intensified Plasma-Assisted Processing, IPAP, is a technique recently developed in our laboratory [1–5]. The process utilizes a triode configuration to produce an intensified glow discharge, which produces a highly energetic particle flux at relatively low pressures and temperatures, with the current density controlled independently of other process parameters, such as bias voltage and pressure. This technique can be used for the synthesis of a large number of compounds and diffusion layers. Most of our recent work has been concentrated on nitriding, where significantly higher effective nitrogen diffusivities were observed compared to the low energy diode method. Similar effects have been previously observed during low-energy ion beam processing [6]. While it is recognized that the energetic particle (ions and neutrals) bombardment and the nature of the layer established at the surface are of utmost importance to the nitriding process, very little information is currently available on these issues.

In this work, the structure of the outer layer formed by plasma nitriding has been analyzed, in order to improve our understanding of the nature of the nitriding mechanism and the role of the energetic particle bombardment in intensified glow discharge nitriding. Several specimens were nitrided at different processing conditions that provided a wide variation in average flux energy in order to investigate the role of the energetic particle bombardment on the nitriding process. Following that, the nitrided surfaces were characterized by X-ray Absorption Spectroscopy (XAS) in both the XANES (X-ray Absorption Near Edge Structure) and EXAFS (Extended X-ray Absorption Fine Structure) regions to provide information about the local structure around titanium atoms in the surface layer. The cross-sections of the modified surface layers were studied by Auger spectroscopy to obtain nitrogen concentration profiles and by electron microscopy for fracture analysis of the processed samples.

2. Experimental

2.1. Specimen preparation by energetic particle bombardment

In this study, two groups of commercially pure titanium specimens were nitrided under different conditions in order to investigate the effect of energetic flux on the nitriding process. All specimens were polished with 1 μm alumina powder as the final step, ultrasonically cleaned in methanol, and dried in air prior to surface treatment.

The first group included five Ti specimens that were processed with an intensified glow discharge, i.e. using

TABLE I Plasma nitriding parameters, calculated energies and doses

Sample	Pressure, Pa	Current density, mA/cm^2	L/λ	E_i^a, eV	E_n^a, eV	Ion dose[a] $\times 10^{20}$	Neutral dose[a] $\times 10^{20}$	Total dose[a] $\times 10^{20}$
I1	6.65	0.5	5.25	616	263	0.3	1.8	2.1
I2	6.65	1.0	3.72	793	325	0.7	2.5	3.2
I3	6.65	1.5	3.04	905	361	1.0	3.1	4.1
I4	6.65	2.5	2.35	1045	406	1.7	3.9	5.6
I5	6.65	3.0	2.16	1077	428	2.0	4.3	6.3
D1	22.61	0.5	17.90	211	100	0.3	6.0	6.3
D2	38.57	1.0	21.60	177	84	0.7	14.6	15.3
D3	49.21	1.5	22.50	170	81	1.0	22.7	23.7

[a]Particles/cm^2

IPAP nitriding. These were prepared at cathode current densities ranging from $i_1 = 0.5$ mA/cm^2 to $i_5 = 3.0$ mA/cm^2, at a pressure $p = 6.65$ Pa (50 mTorr) and bias voltage $V_c = 2000$ V. The second group included three specimens that were nitrided at lower plasma energy conditions, using the IPAP system in the diode mode. This group was processed at the same bias voltage as the previous specimens, with the cathode current density controlled between $i_6 = 0.5$ mA/cm^2 and $i_8 = 1.5$ mA/cm^2 by adjusting the chamber pressure. A processing time of three hours was used for all samples.

The processing parameters for both groups of specimens are summarized in Table I. The sample numbers begin with "I" (intensified) for the samples prepared with the triode discharge and "D" for the samples prepared with the diode discharge. This choice of processing parameters resulted in a wide range of values for the average ion (E_i^a) and neutral (E_n^a) energies. These energies were calculated following the procedure outlined in a previous publication [5]. It is worth noting that the energies are mainly a function of the L/λ ratio where L is the dark space length and λ the mean free path for charge exchange collisions. Low values of L/λ pertain in intensified discharge ($L/\lambda < 10$) resulting in higher flux energies compared to the diode process ($L/\lambda > 10$). Also, it should be noted that current densities for the diode treatments were not increased beyond 1.5 mA cm^{-2} since higher flux energies can not be achieved. Higher current densities for the diode treatment can be obtained only by increasing the system pressure, but this results in lower particle energies, Table I.

2.2. Analysis of surface layers

Concentration profiles of chemical elements present in the nitrided layer and fracture characteristics were studied using a JAMP-10 S (JEOL-JAPAN) Auger spectrometer. The spectrometer was modified to allow fracturing of specimens under vacuum. Nitrided specimens were sectioned from the side opposite the nitrided surface leaving only a thin material layer that was subsequently fractured in the chamber. Fracture surfaces were then studied with electron microscopy. Fracturing the samples in the work chamber at very low pressure (5×10^{-8} Pa) provides a "clean" surface, without adsorbed atoms and molecules of O, C, N, etc. The e-beam scanning system and appropriate detectors used with the system allow surface imaging with Auger and secondary electrons with 250 Å resolution. In the Auger-electron microscopy mode, the characterized area is below 1 μm in diameter at a primary beam current of 10^{-6} A–10^{-7} A and bias voltage 10 kV.

Sputtering of the characterized surfaces with an ion gun was used for depth profile analysis of the samples. An Ar^+ beam with an energy of 3 keV was focused on the specimen to produce a spot size of about 2 mm for sputtering.

XAFS spectra at the K edge of titanium (4966 eV) were recorded at the Center for Advanced Microstructures and Devices (CAMD), Louisiana State University. Data were collected using bending, magnet radiation ($E_c = 2.6$ keV) at the DCM1 beamline where the X-ray beam was monochromatized with a fixed exit double crystal monochromator operating with Si(111) or Ge(220) crystals. The incident monochromatic X-ray intensity (I_0) was monitored with an ionization chamber filled with one atmosphere of air and XAFS spectra were recorded in total electron yield (TEY) mode, with one atmosphere of helium in the detector chamber [7]. EXAFS spectra were recorded over an energy range of 4800–5970 eV with 1 eV steps; XANES spectra were recorded from 4910–5400 eV with 0.2 eV steps in the near edge region. The TEY and I_0 detector signals were divided (TEY/I_0) to yield the raw spectral data.

XANES data were fitted with a linear pre-edge for background removal and normalized to the 5300–5400 eV post-edge regions of the spectra. The pure Ti metal and TiN standard spectra were used to model the experimental sample spectra by linear combination using the WinXAS software package [8]. The XANES fitting was performed over the region 4950–5000 eV. The EXAFS spectra were extracted and analyzed utilizing the UWXAFS software package [9]. Background removal and normalization were performed using the AUTOBK routine in the UWXAFS package. E_0 was set at the first inflection point of the Ti metal spectrum, and the extracted EXAFS signal was Fourier transformed over the region of 2.5 Å^{-1} to 11 Å^{-1} using a Hanning window function. For detailed analysis, the fractional contribution of Ti metal (as determined by the

linear combination XANES analysis) was subtracted from the extracted EXAFS signal, and the spectrum was re-normalized and Fourier transformed as above. Refined structural parameters were obtained from non-linear least square fitting in R-space over a range of 1.2 Å to 3 Å, encompassing the first two peaks representing Ti. . .N and Ti. . .Ti, in the single scattering approximation. Theoretical phase and amplitude functions for TiN were calculated using FEFF6, a computer program for *ab initio* calculation of EXAFS and XANES spectra using multiple-scattering theory [10]. The amplitude reduction factor S_0^2 was determined by fitting the EXAFS data of the TiN powder standard, yielding a value of 0.634.

3. Results and discussion

3.1. AES and SEM surface analysis

The nitrided specimens fractured in the working chamber exhibited, in general, two modes of fracture. A mainly ductile transgranular fracture typical for titanium was observed for the entire specimen fracture surface except for the IPAP treated specimens. The latter specimens exhibited a brittle surface layer, evidenced by the multiple cracking present at the surface region, that was not present in the diode treated specimens, Fig. 1. The latter fracture surface was characterized by ductile, dimpled morphology similar to that in the bulk. This brittle layer, seen in the top part of Fig. 1a, very likely includes both TiN and Ti_2N layers that are

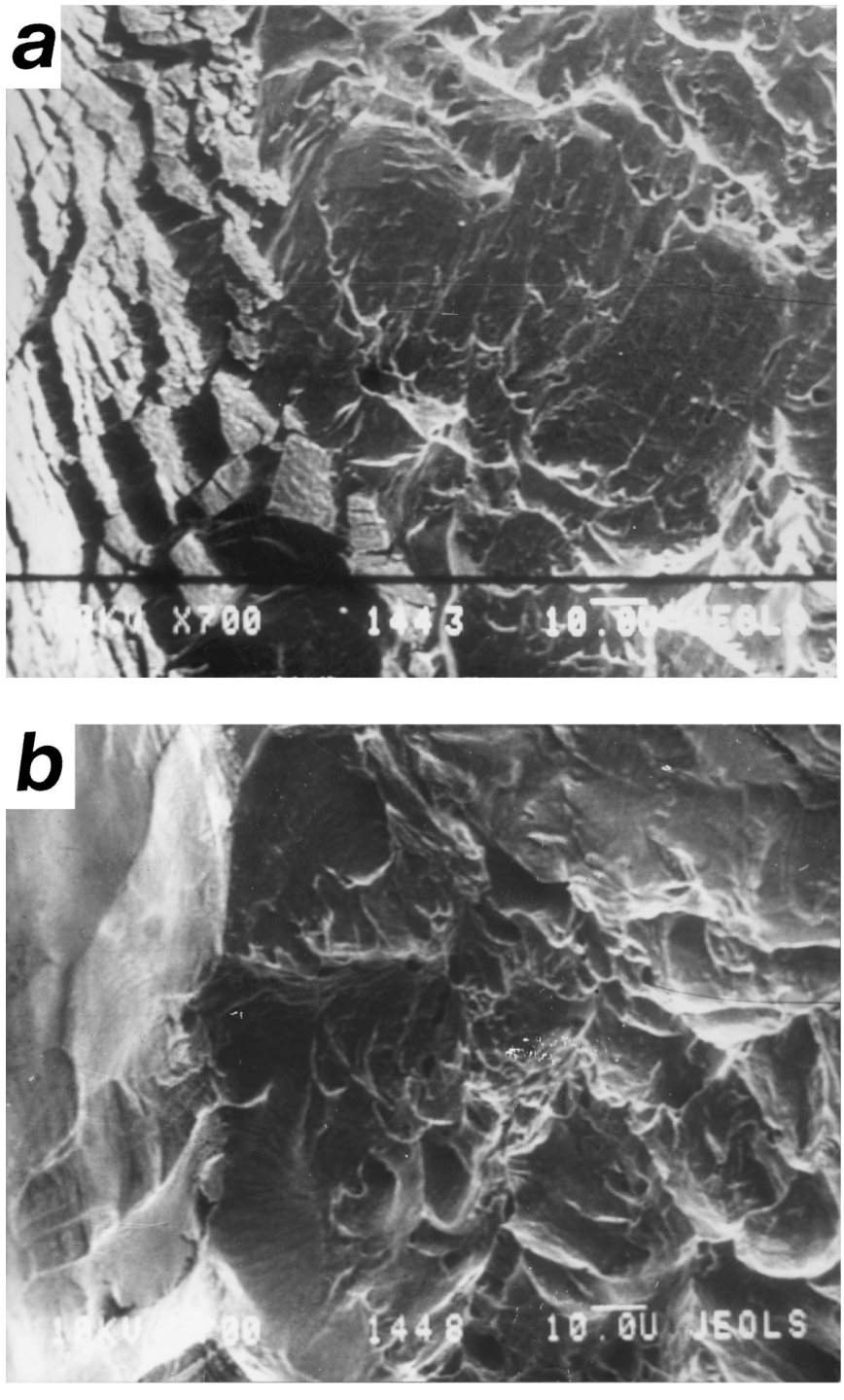

Figure 1 Scanning electron micrograph of fracture surface of plasma nitrided specimen (a) IPAP 1 mA/cm^2 and (b) diode 1 mA/cm^2.

expected to form during IPAP nitriding of Ti [3]. The layer thickness was estimated to be approximately 3–5 μm. It should be noted that no brittle layer could be detected in the specimens of the second group, Fig. 1b, either because it was not present or was very thin. As can be expected, IPAP samples show effects of plasma etching, which become more pronounced as the bombarding particle energies are increased, Figs 2a and b. Samples of the second group, processed by diode plasma nitriding, exhibit relatively smooth surfaces without significant traces of sputtering as a result of the lower energy bombardment pertaining in this process, Fig. 2c.

The composition depth profiles of the processed specimens were measured by AES. Relative intensities were determined from peak-to-peak heights and elemental concentrations were calculated from

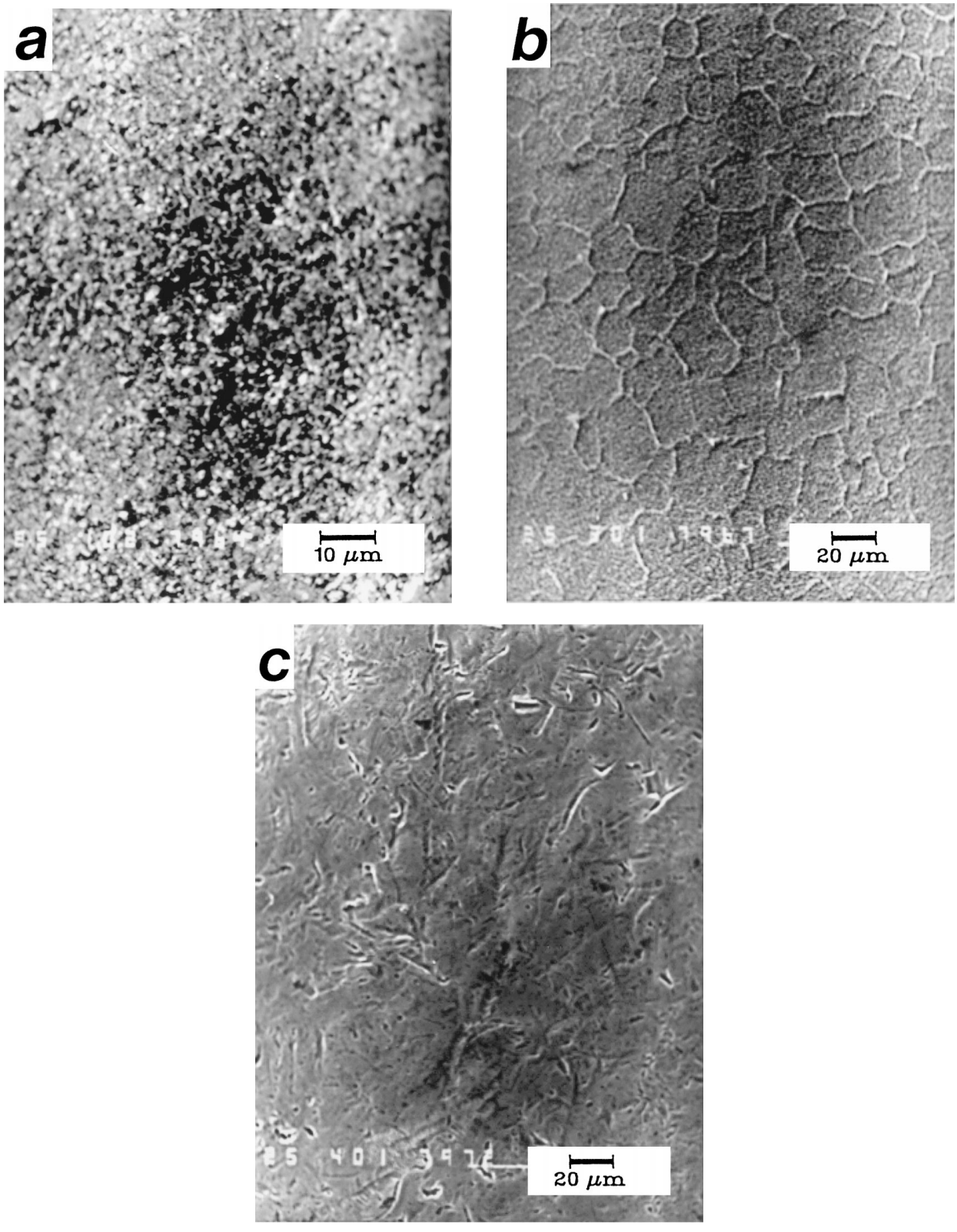

Figure 2 Scanning electron micrograph of nitrided surfaces of specimens treated with (a) IPAP 1 mA/cm^2, (b) IPAP 2.5 mA/cm^2, and (c) diode 1 mA/cm^2.

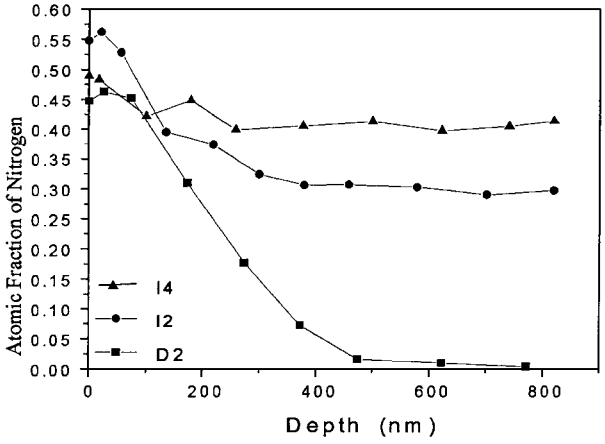

Figure 3 Nitrogen concentration profiles measured by AES.

these intensities by using the appropriate sensitivity factors. Fig. 3 shows nitrogen concentration profiles for two IPAP samples prepared with current densities of 1 mA/cm^2 and 2.5 mA/cm^2 and one conventionally processed sample prepared at 1 mA/cm^2. As can be seen from Fig. 3, the nitrogen content at the surface is approximately 50 at.% for all samples. For the sample prepared with the diode nitriding process, the nitrided layer is very thin (<500 nm), with the nitrogen content decreasing rapidly with increasing depth. For the IPAP samples, the nitrided layer extends well beyond the measured range (>800 nm), in spite of the fact that the dose for these samples was considerably lower compared to that of the diode treatment, Table I. Also, in view of the calculated energies, Table I, the AES results suggest an energy dependence of the nitriding depth.

3.2. EXAFS

Fig. 4 shows normalized spectra of the XANES region and part of the EXAFS region for Ti metal, TiN powder, and IPAP samples I1, I3, and I5. This shows clearly the overall trend observed for these samples. Sample I1 (low current density, low energy) produced a spectrum which is very similar to that of Ti metal (both in the near edge structure and in the EXAFS region); sample I5 (high current density, high energy) produced a spectrum which matches well with that of TiN; the intermediate samples appear to be a mixture, with the fraction of TiN signal increasing with the current density. In Fig. 5, a similar comparison is made for the diode glow discharge samples. In this case a point is never reached at which the spectrum closely resembles that of TiN.

Fig. 6 concentrates on the XANES region of the spectrum for the same IPAP samples that are shown in Fig. 4. The Ti metal spectrum exhibits a sharp pre-edge feature at 4966 eV (generally attributed to a transition to a 3*d* state with strong *p* hybridization [11]). This pre-edge feature does not appear in the TiN spectrum, which is characterized by a strong "white" line at 4984 eV. Also, the absorption edge for TiN is shifted to a higher energy relative to Ti metal, consistent with the difference in Ti oxidation state between Ti metal (Ti^0) and TiN (Ti^{2+}). In the IPAP samples the trend from a Ti metal-like to a TiN-like spectrum as a function of current density can

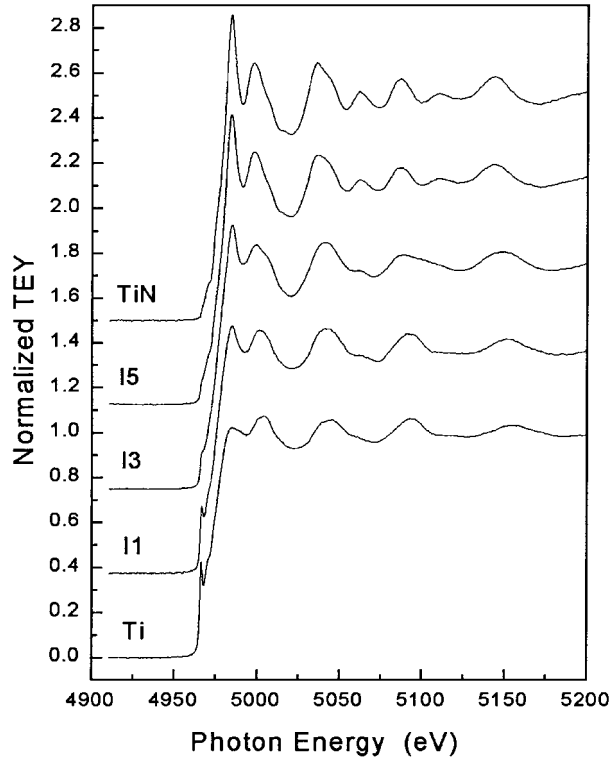

Figure 4 Normalized XAS of IPAP samples.

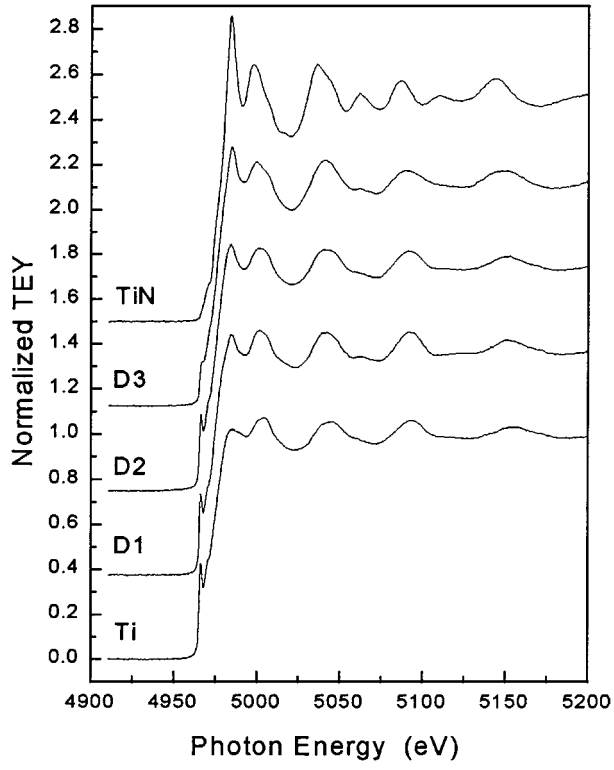

Figure 5 Normalized XAS of diode samples.

be followed, with the intensity of the Ti metal pre-edge feature decreasing and the intensity of the TiN white line increasing as current density increases. It is, therefore, reasonable to attempt to model these spectra as two-phase mixtures of Ti and TiN. The XANES spectra for the samples nitrided with the conventional diode system are presented in Fig. 7. Again, a trend can be observed with the Ti pre-edge feature decreasing and

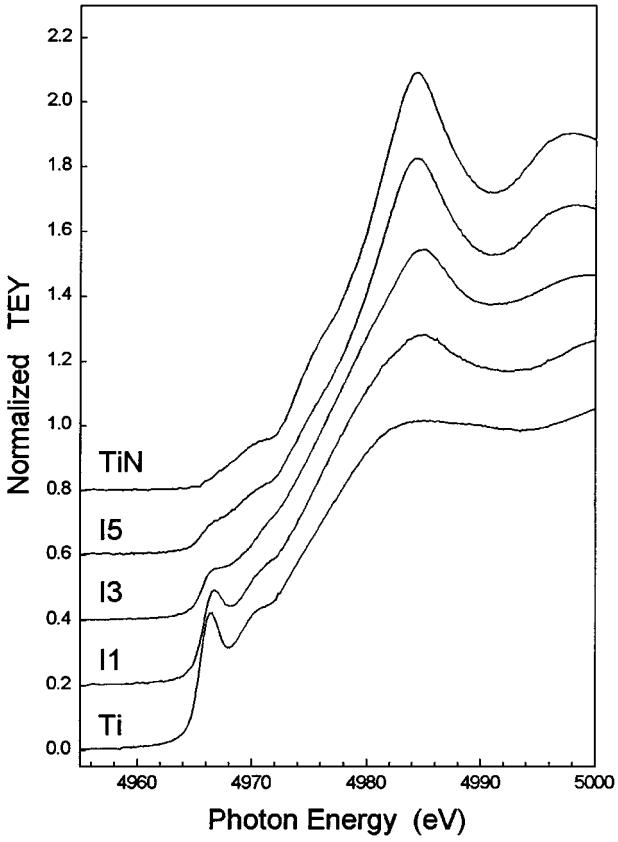

Figure 6 XANES of IPAP samples.

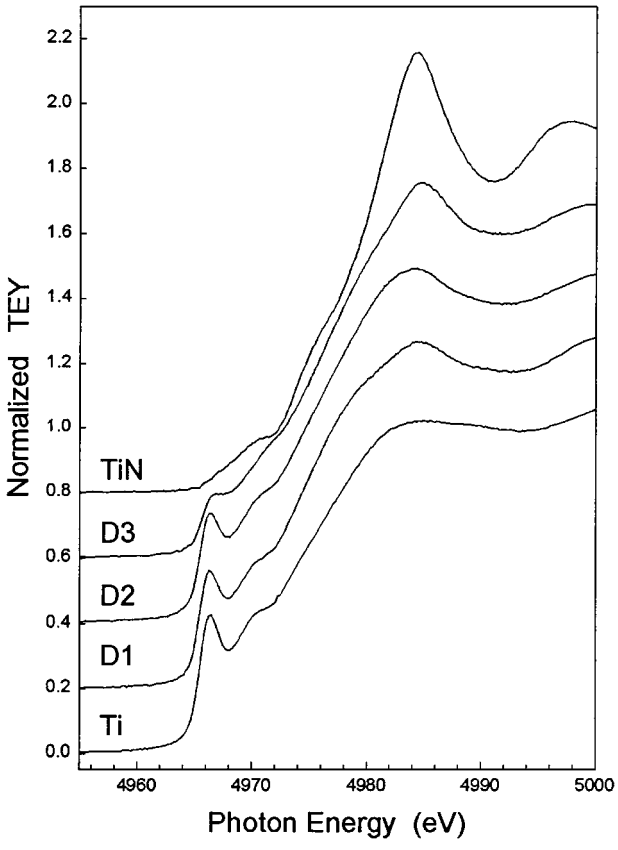

Figure 7 XANES of diode samples.

the white line increasing with current density. Least-squares fitting of the XANES spectra as a linear combination of the spectra of the component phases Ti and TiN was used to gain quantitative information of the phase fractions. Linear combination XANES fits were performed on the spectra over the region 4950–5000 eV that covers the Ti metal pre-edge feature and the TiN white line. The results are presented in Table II and plotted in Fig. 8. For the high energy IPAP samples (I4 and I5), very good fits were obtained, with the system consisting mainly of TiN. Since the two-component model gave good fits to the data, it is taken as a valid model for the surface structure of these samples. For the lower energy IPAP samples and for the diode samples, less TiN was found in the fits, and the residuals and quality of fit factors were not as good. This could be due to the presence of another phase (Ti_2N) or distortion of the α-Ti XANES due to high amounts of interstitial nitrogen. In any case, the fits are a measure of the decrease in the Ti metal pre-edge feature and the corresponding growth of the TiN white line and therefore serve as a good indicator of the overall amount of nitriding.

It should be noted that the amount of nitrogen determined by AES at the surface region is significantly higher than that present in the TiN phase as determined by XANES spectroscopy. This is more than likely due to the fact that AES cannot distinguish between nitrogen bonded to Ti and nitrogen in interstitial positions or at grain boundaries.

TABLE II TiN fraction obtained by XANES linear combination fitting

Sample	Current density, mA/cm^2	%Ti	%TiN	r-factor	χ^2 $\times 10^5$
I1	0.5	74.7	25.3	1.0	0.63
I2	1.0	56.3	43.77	1.15	9.47
I3	1.5	47.8	52.2	1.27	3.9
I4	2.5	21.7	78.3	0.51	0.10
I5	3.0	18.1	81.8	0.52	0.099
D1	0.5	86.6	13.55	1.0	5.0
D2	1.0	77.5	22.5	0.8	1.6
D3	1.5	56.2	43.8	1.1	3.3

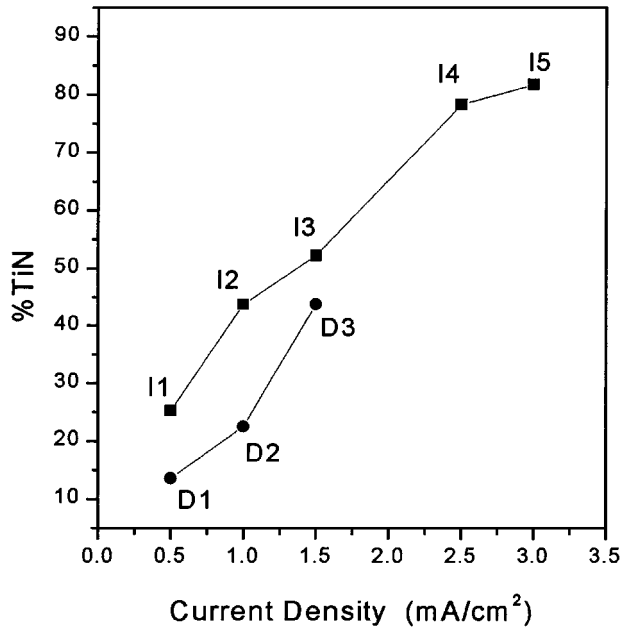

Figure 8 Phase fractions based on XANES fits.

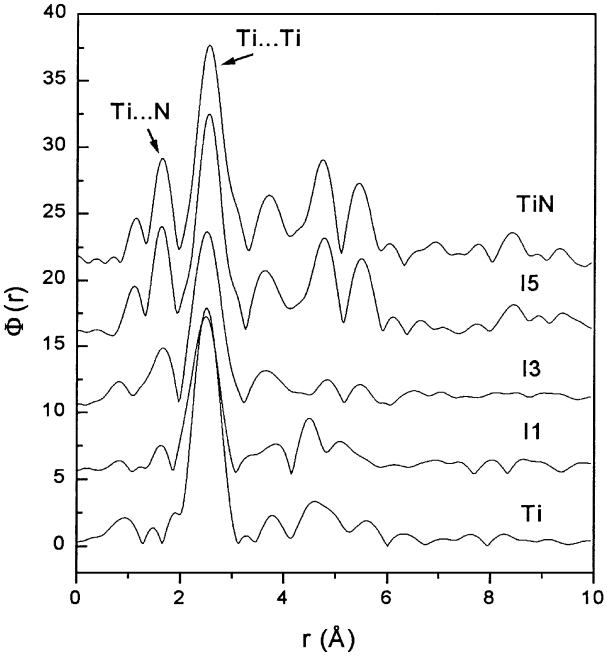

Figure 9 EXAFS-FT of IPAP samples.

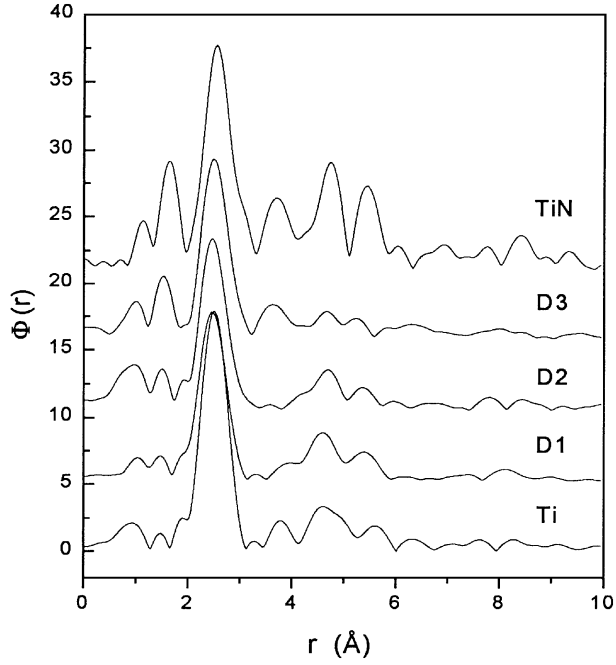

Figure 10 EXAFS-FT of diode samples.

EXAFS Fourier transforms of Ti metal, TiN, and the I1, I3, and I5 IPAP samples are shown in Fig. 9. The TiN powder and the I5 IPAP nitrided sample transforms are very similar, exhibiting peaks at ∼1.75 Å and ∼2.70 Å (the Fourier transforms are not phase corrected), which can be assigned to Ti. . .N and Ti. . .Ti nearest neighbor interactions at 1.96 Å and 2.99 Å respectively. Also, the 3.5 Å to 6.0 Å regions of these transforms are very similar indicating that the longer distance interactions may be equivalent. The 1.5 mA/cm^2 and 0.5 mA/cm^2 IPAP nitrided sample Fourier transforms also exhibit peaks at ∼1.75 Å and ∼2.70 Å. A clear trend can be observed, with the amplitude of the peak at ∼1.75 Å (representing the Ti. . .N interaction) gradually increasing with current density. The peak at ∼2.70 Å remains at full amplitude throughout the series of samples, and can be modeled by a Ti. . .Ti interaction with a coordination number of 12, which would be observed in both the Ti metal and TiN structures. The 3.5 Å to 6.0 Å regions in the 1.5 and 0.5 mA/cm^2 IPAP samples (I1 and I3) do not show an obvious match to either Ti metal or TiN, indicating a mixed or intermediate structure. From these transforms, as from the XANES spectra, the main observation is that the surface structure becomes more like that of pure TiN with increasing current density (which corresponds to an increase in particle energy). The Fourier transforms for the conventional samples are presented in Fig. 10. A similar increase in nearest-neighbor nitrogen is observed with increasing current density, but the nitrogen interaction peak does not approach the intensity observed in TiN.

A detailed analysis of the EXAFS data could be performed to extract structural parameters for the nearest neighbor distances, coordination numbers, Debye-Waller factors, etc. However, since the XANES spectra indicate the presence of a multiphase system, parameters extracted from the averaged signal would be of limited value. Instead, EXAFS analysis was used to test the two-phase model. This was done by subtracting the Ti metal contributions determined by the XANES analysis (Table II) from the extracted EXAFS signal. For example, the XANES analysis of the 3.0 mA/cm^2 IPAP sample (I5) indicated the sample to be 18% Ti metal and 82% TiN. The extracted EXAFS signal for the Ti metal standard was therefore multiplied by 0.18, and the result was subtracted from the extracted EXAFS signal for the sample. The resultant EXAFS spectrum was normalized (multiplied by 1/0.82). EXAFS Fourier transforms of the Ti metal subtracted sample spectra are shown in Fig. 11, along with Fourier transforms of TiN and Ti metal. The TiN and I5 Fourier transforms are virtually identical, and the I3 IPAP sample Fourier transform is very similar. Fitting of the first two shells using FEFF phase and amplitude functions

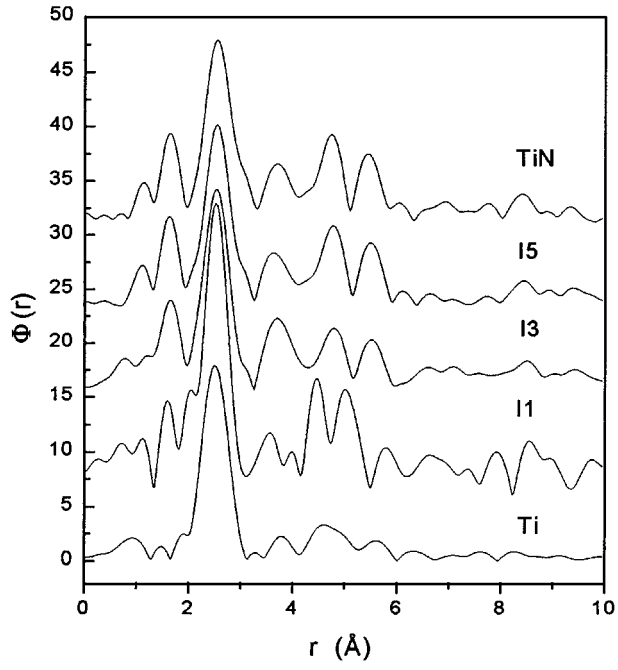

Figure 11 EXAFS-FT after subtracting Ti metal.

TABLE III Coordination numbers and distances obtained from EXAFS fitting. [ΔE_0 and σ's for all samples obtained from TiN powder sample: $\sigma_{\text{Ti-N}} = 0.0027$, $\delta_{\text{Ti-Ti}} = 0.0050$; $\Delta E_{\text{Ti-N}} = 3.5$ eV, $\Delta E_{\text{Ti-Ti}} = -0.88$ eV]

Sample	Current density mA/cm^2	n_{N}	r (Å)	n_{Ti}	r(Å)
I1	0.5	—	—	—	—
I2	1.0	6.27 ± 1.1	2.104 ± 0.004	13.9 ± 1.0	2.976 ± 0.004
I3	1.5	6.39 ± 1.0	2.099 ± 0.004	13.1 ± 0.9	2.968 ± 0.004
I4	2.5	5.4 ± 1.0	2.105 ± 0.005	10.7 ± 0.9	2.978 ± 0.005
I5	3.0	5.8 ± 0.5	2.115 ± 0.002	11.8 ± 0.4	2.992 ± 0.002

was performed as described above. For the I5 IPAP sample, a good fit was obtained with parameter values very close to those of the TiN standard. The σ^2 values obtained for the TiN powder were used in the fits and it was not necessary to vary them to achieve an acceptable fit. The Ti. . .N and Ti. . .Ti coordination numbers (N) are in good agreement with those of stoichiometric TiN, and so are the fit-determined distances (R). The analysis indicates the presence of a well ordered stoichiometric TiN phase. The fact that subtracting the Ti metal signal contribution leaves essentially a pure TiN signal strongly supports the two phase model, and it is concluded that the 3.0 mA/cm^2 IPAP sample (I5) consists (at the surface) of TiN, and a small amount of Ti metal, with other phases present only in minor amounts, if at all. As can be seen in Table III, similar results were obtained in fitting the 1.0 through 2.5 mA/cm^2 IPAP samples. For the 0.5 mA/cm^2 sample I1, the Ti metal/TiN two phase model breaks down (no good fits based on TiN could be obtained from the Ti metal subtracted EXAFS), suggesting the possible presence of some other phase. Possibilities include Ti_2N or an amorphous phase, but there is no direct evidence of their presence. Attempts to perform such analysis on the data from the diode samples were unsuccessful, as in the I1 sample.

Based on the XANES and EXAFS analysis, we can see the effect of the processing parameters on the surface structure of nitrided samples. It is clear that at high particle energies achieved in IPAP, well ordered stoichiometric TiN can be formed at the surface, with the amount (phase fraction) of TiN increasing with current density. This effect cannot be achieved at lower particle energies utilized in the diode glow discharge nitriding.

4. Conclusions

The present results showed that higher bombarding particle energies during plasma nitriding promote the formation of a continuous TiN surface layer. In spite of the significantly higher dose pertaining in the diode process, low energy bombardment produces a small amount of the TiN phase in the near surface region. Based on EXAFS and XANES results a two-phase model for the outer layer was proposed and quantitatively tested. The model was found to be in good agreement with the experimental data especially for specimens treated at high bombarding particle energies.

Acknowledgements

This work was supported by the Army Research Office (Grant Number: DAAG55-98-1-0279), the Louisiana Board of Regents and CAMD.

References

1. J. XU and E. I. MELETIS, in "Beam Processing of Advanced Materials," edited by J. Singh and S. M. Copley (The Metallurgical Society, Warrendale, PA, 1993), p. 551.
2. E. I. MELETIS and S. YAN, *J. Vac. Sci. Technol.* **11**(1) (1993) 25.
3. T. M. MURALEEDHARAN and E. I. MELETIS, *Thin Solid Films* **221** (1992) 104.
4. E. I. MELETIS and S. YAN, *J. Vac. Sci. Technol.* **9**(4) (1991) 2279.
5. A. ADJAOTTOR, E. MA and E. I. MELETIS, *Surf. Coat. Technol.* **89** (1997) 197.
6. D. L. WILLIAMSON, O. OZTURK, R. WEI and P. J. WILBUR, *ibid.* **65** (1994) 15.
7. G. TOURILLON, E. DARTYGE, A. FONTAINE, M. LEMONNIER and F. BARTOL, *Phys. Lett. A*, **121** (1987) 251.
8. T. RESSLER, *J. Physique IV*, **7** (1997) C2-269.
9. E. A. STERN, M. NEWVILLE, B. RAVEL, Y. YACOBY and D. HASKEL, *Physica B*, 208–209 (1995) 117.
10. J. J. REHR, J. MUSTRE DE LEON, S. I. ZABINSKY and R. C. ALBERS, *J. Amer. Chem. Soc.* **113** (1991) 5135.

Received 5 August 1998
and accepted 9 September 1999